Published in IET Electrical Systems in Transportation
Received on 17th October 2011
Revised on 18th June 2012
doi: 10.1049/iet-est.2011.0051

ISSN 2042-9738

Fault location for aircraft distribution systems using harmonic impedance estimation

Q. Zhou M. Sumner D. Thomas

Department of Electronic and Electrical Engineering, University of Nottingham, Nottingham NG7 2RD, UK
E-mail: qian.zhou@nottingham.ac.uk

Abstract: The demands for 'more electric aircraft' will increase the power distribution requirements of future aircraft electrical distribution systems. To increase safety and reduce aircraft maintenance times on the ground, there is also a need for system condition monitoring to quickly identify and locate any electrical faults which may develop. The work presented in this study forms an initial study into the use of power system harmonic impedance measurement for identifying and locating faults within power cables. The method is passive – that is, it does not require the injection of any test signals – and can be embedded into a centralised equipment controller to provide intelligent, real-time diagnostics. The method estimates the harmonic line–line self-impedance at strategic points in the distribution system by measuring load voltage and current at different load distribution points within the network. By combining the harmonic line–line self-impedance estimates the faults can be identified and located within a few cycles. This can, therefore, provide a 'backup protection' system, which does not require bus current measurement. It can also provide a measure of the fault location and could therefore be a significant aid to aircraft maintenance. The study derives the theoretical basis of the scheme and provides experimental results from a laboratory prototype to demonstrate the validity of this approach to detect and locate faults within the system.

1 Introduction

For conventional aircraft, fuel is converted into propulsive power to move the aircraft, and four main forms of non-propulsive power: pneumatic power, mechanical power, hydraulic power and electrical power [1–5] are generated. The concept of 'all electric aircraft' or 'more electric aircraft' (MEA) has been introduced to reduce the use of hydraulic and pneumatic power, thereby bringing advantages such as improved fuel consumption and lower maintenance and operation costs [1].

The increased reliance on electrical energy in an MEA puts increased stress on the protection and control systems, increasing the electrical energy distributed from a few hundred kW to over a MW for a 737 sized aircraft [6]. Improved fault identification and location is important to enable the electrical power systems to meet the increased load demand and functionality. The protection mechanisms are indispensable for any power system and are well established for distribution/transmission systems. The protection techniques for distribution lines can be generally classified into two categories: the non-unit-type (such as distance protection and over-current relays) and unit-type protection [7]. Owing to the short length of the cable in an aircraft power system, distance fault detection schemes or time graded over-current relays are unsuitable. The current differential protection scheme, one of the unit protection schemes, have been successfully applied to protect distribution lines [8] as they can be set to operate rapidly, if low-current internal faults occur and they provide the capability of discriminating between faults internal and external to the protected zones [9]. However, the extra communication channel or pilot wires required make them too cumbersome for many aircraft applications. Most protection on aircraft systems will therefore comprise simple over-current relays without any fault location capability. In recent years, there has been an increased research focus on developing reflectometry methods for locating faults on aircraft wiring [10]. The reflectometry methods are techniques usually used for testing ageing wires and identifying wiring faults. There are several types of reflectometry-based algorithms used for this application, such as time domain reflectometry [11], frequency domain reflectometry [12, 13], sequence time domain reflectometry [14, 15] and spread spectrum time domain reflectometry (SSTDR) [14, 16–18]. Hard faults (open and short-circuit) can be detected by these reflectometry techniques, but soft faults, such as damaged insulation, are not generally observable. S/SSTDR methods can be applied for locating intermittent faults or running real-time testing of live wiring systems [10]. However, these methods have mainly been applied to communication wiring looms.

Intelligent electronic devices (IED) that can be applied for data acquisition, protection and control, are primarily applied to the digital monitoring and protection of power system equipment such as transmission/distribution lines, switchgear, buses and transformers [19–21]. The IED relays designed for protecting distribution lines have to meet different requirements for providing both primary

and backup protection [20]. Many different associated fault detection functions, such as distance protection [9] and directional protection [9] have been developed and can be integrated into the IEDs to provide backup protection schemes. In this paper, a novel fault detection and location scheme using the THLSI is proposed. It can potentially be integrated into an IED relay to provide information in addition to that provided by the primary protection system to assist with the accurate determination of the fault location.

Impedance measurement is one of the common techniques used in relay protection [9], and therefore its principle is considered here. The new method monitors the third harmonic line–line self-impedance (THLSI) at strategic points in the distribution system; this is obtained by measuring voltage and current at the load distribution centres. The THLSI has been chosen specifically as it is a function of the lowest (largest) triplen harmonics and changes significantly in the presence of asymmetry, especially a fault condition. If a fault occurs, the new method can provide accurate fault identification and location, without direct measurement of the main bus currents. It therefore could provide a backup protection signal, as well as information on fault location for maintenance. However, it is important to note that the THLSI at load distribution centres can be calculated relatively easily. This can potentially be achieved by enabling simple software modification to the remote electronic units (REUs) already deployed at the load distribution centres, and therefore this additional information can be obtained at a relatively small extra cost. This information would help a centralised controller to quickly reconfigure the distribution system, and maintain supply to essential loads in the presence of cabling faults, and also reduce the maintenance time on the ground by providing an accurate indication of fault location.

This paper describes the use of the THLSI for fault location. The parameter is derived in Section 2 and shown to be related to both fault location and fault severity. Section 3 introduces an experimental rig based on the simplified aircraft electric distribution system described in [5]. Two sets of fault scenario are tested, and a fault location algorithm based on the THLSI measured at the load distribution centres is demonstrated, followed by a discussion of the proposed method in Section 4 and the conclusions in Section 5. Simulation work has verified the validity of this new algorithm [22, 23]. This paper provides a more extensive theoretical background to the new method, together with experimental validation.

2 Principle of line–line self-impedance for fault location

2.1 Overview

In a practical distribution system, the grid voltages will become polluted with harmonics and inter-harmonics because of the effects of non-linear loads. Therefore the phase–ground or phase–phase voltage and the line currents in a three-phase system are the sum of sinusoidal functions at the fundamental, harmonic and inter-harmonic frequencies. For the three-phase three-wire topology proposed for MEA systems, the instantaneous phase–phase voltages at the load distribution centres are related to the instantaneous line currents flowing to the loads by (1), if the loads are star connected.

$$\begin{cases} v_{ab} = i_a Z_a - i_b Z_b \\ v_{bc} = i_b Z_b - i_c Z_c \\ v_{ca} = i_c Z_c - i_a Z_a \end{cases} \tag{1}$$

where Z_a, Z_b and Z_c are the per phase load impedance and i_a, i_b and i_c are the load currents. Equation (2) presents the frequency domain representation of (1), where $F(\cdot)$ denotes the Fourier transform

$$\begin{cases} F(v_{ab})_\omega = Z_a(\omega)F(i_a)_\omega - Z_b(\omega)F(i_b)_\omega \\ F(v_{bc})_\omega = Z_b(\omega)F(i_b)_\omega - Z_c(\omega)F(i_c)_\omega \\ F(v_{ca})_\omega = Z_c(\omega)F(i_c)_\omega - Z_a(\omega)F(i_a)_\omega \end{cases} \tag{2}$$

Dividing (2) by the Fourier coefficients of the related line-currents yields (3).

$$\begin{cases} Z_{ab}(\omega) = \dfrac{F(v_{ab})_\omega}{F(i_a)_\omega} = Z_a(\omega) - Z_b(\omega)\dfrac{F(i_b)_\omega}{F(i_a)_\omega} \\ Z_{bc}(\omega) = \dfrac{F(v_{bc})_\omega}{F(i_b)_\omega} = Z_b(\omega) - Z_c(\omega)\dfrac{F(i_c)_\omega}{F(i_b)_\omega} \\ Z_{ca}(\omega) = \dfrac{F(v_{ca})_\omega}{F(i_c)_\omega} = Z_c(\omega) - Z_a(\omega)\dfrac{F(i_a)_\omega}{F(i_c)_\omega} \end{cases} \tag{3}$$

The left-hand terms of (3) are defined as the 'line–line self-impedance' at the load terminal in the frequency domain. The 'line–line self-impedance' at the third harmonic frequency has been chosen to indicate unbalance and fault levels within the system for the reasons detailed as follows:

If a three-phase non-linear load is connected to the system, for example, an inductively or capacitively smoothed rectifier, then under normal operation, harmonic currents will be produced by the non-linear load at harmonic frequencies of $6n \pm 1$, where n is an integer [24]. The magnitude of the harmonic current component reduces with frequency [25]. When an asymmetric fault occurs, other harmonic currents (especially the non-even triplen harmonics) are introduced. This is because, the voltage applied to the input terminal of the non-linear load is now unbalanced. A full description of how these non-even triplen harmonics currents are produced is provided in [25]. The current distortion at these harmonics is dependent on the degree of unbalance. The magnitude of the third harmonic current is large compared with the other triplen harmonics, and therefore the third harmonic is selected to maximise the signal-to-noise ratio (SNR) of any measurements made.

2.2 Fault location using self-impedance

In order to illustrate how the concept of 'line–line self-impedance' can be applied to detect and locate faults within the system, an example network has been analysed. When a phase–phase short-circuit fault occurs within the system, the diode rectifier will create triplen harmonics currents that are injected onto the network. Fig. 1 depicts the equivalent circuit of the example network at harmonic frequencies. In the example network, the internal impedance of the supply source is $Z_s(R_s,\ X_s)$ and its admittance is $Y_s(Y_s = 1/Z_s)$. The impedance of the passive load connected at Node 1 is $Z_1(R_1,\ X_1)$ and its admittance is $Y_1(Y_1 = 1/Z_1)$. The impedance and admittance of the power bus cable for the length from the fault location back to the supply source terminal are denoted as Z_{Tx} and Y_{Tx} $(Y_{Tx} = 1/Z_{Tx})$,

doi: 10.1049/iet-est.2011.0051

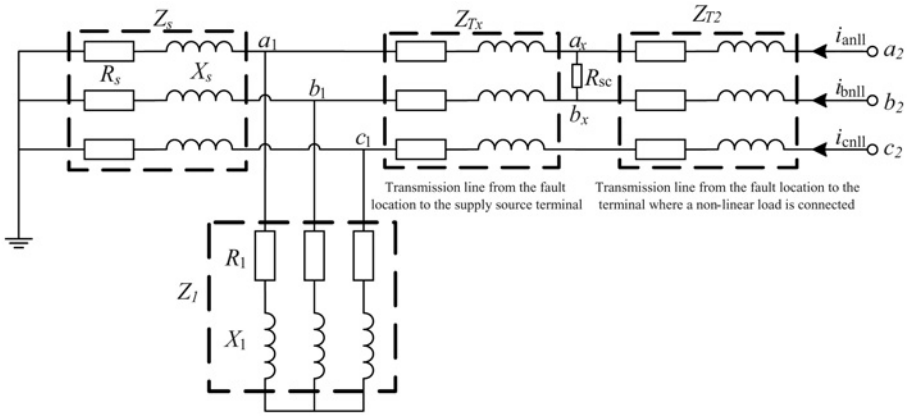

Fig. 1 *Equivalent topological circuit of the example network viewed at the harmonic frequencies*

respectively. The impedance of the power bus cable for the length from the fault location to the non-linear load terminal is denoted as $Z_{T2}$and its admittance is Y_{T2} ($Y_{T2} = 1/Z_{T2}$) The non-linear load is connected at Node 2 (a_2, b_2, c_2).

Equation (4) describes the relationship between the phase voltages at the fault location (v_{ax}, v_{bx}) and the phase voltages at the passive load (Node 1 – v_{a1}, v_{b1}) using the relevant admittances.

$$\begin{cases} (v_{ax} - v_{a1})Y_{Tx} = v_{a1}(Y_s + Y_1) \\ (v_{bx} - v_{b1})Y_{Tx} = v_{b1}(Y_s + Y_1) \end{cases} \tag{4}$$

From (4), the phase voltages at the fault location can be expressed by

$$\begin{cases} v_{ax} = \left(1 + \dfrac{Y_s + Y_1}{Y_{Tx}}\right)v_{a1} \\ v_{bx} = \left(1 + \dfrac{Y_s + Y_1}{Y_{Tx}}\right)v_{b1} \end{cases} \tag{5}$$

The harmonic currents at the non-linear load can also be related to the phase voltages at the fault location and the passive load terminal by the relevant admittances, as shown in (6), where R_{sc} is the fault resistance.

$$\begin{cases} i_{anll} = (v_{ax} - v_{a1})Y_{Tx} + (v_{ax} - v_{bx})\dfrac{1}{R_{sc}} \\ i_{bnll} = (v_{bx} - v_{b1})Y_{Tx} + (v_{bx} - v_{ax})\dfrac{1}{R_{sc}} \end{cases} \tag{6}$$

substituting (5) into (6), the voltage at the passive load terminal (Node 1) can be expressed by

$$\begin{cases} v_{a1} = \dfrac{1}{A^2 - B^2}(Ai_{anll} + Bi_{bnll}) \\ v_{b1} = \dfrac{1}{A^2 - B^2}(Bi_{anll} + Ai_{bnll}) \end{cases} \tag{7}$$

where the variables A and B in (7) are defined in (8). Both A and B are the function of the fault location and fault resistance, which are represented by the admittance of the transmission line from the fault location back to the network source terminal Y_{Tx} and the short-circuit fault resistance R_{sc}, respectively.

$$\begin{cases} A = Y_s + Y_1 + \left(1 + \dfrac{Y_s + Y_1}{Y_{Tx}}\right)\dfrac{1}{R_{sc}} \\ B = \left(1 + \dfrac{Y_s + Y_1}{Y_{Tx}}\right)\dfrac{1}{R_{sc}} \end{cases} \tag{8}$$

The phase-phase voltage at the passive load (Node 1 in this case) and the line-current flowing to this load can be calculated by the following equations

$$\begin{cases} v_{ab1} = v_{a1} - v_{b1} = \dfrac{i_{anll} - i_{bnll}}{A + B} \\ i_{a1} = \dfrac{1}{Z_1} \cdot \dfrac{1}{A^2 - B^2}(A \cdot i_{anll} + B \cdot i_{bnll}) \end{cases} \tag{9}$$

The aim of the proposed algorithm is to measure the 'line–line self-impedance' at each load distribution centre (Nodes 1 and 2 in this case) at the third harmonic frequency. According to (3), the 'line–line self-impedance' at the passive load (Node 1) at the third harmonic frequency (3ω) can be defined by (10). It is clear that (10) is a function of A and B that is, the fault resistance and its location.

$$\begin{aligned} Z_{ab1}(3\omega) &= \frac{F(v_{ab1})_{3\omega}}{F(i_{a1})_{3\omega}} \\ &= \left\{1 + \frac{Z_1(3\omega)}{Z_s(3\omega)}\right\} \cdot \frac{F(i_{anll})_{3\omega} - F(i_{bnll})_{3\omega}}{(A(3\omega) + B(3\omega)) \cdot F(i_{anll})_{3\omega}} \end{aligned} \tag{10}$$

A similar expression for the 'line–line self-impedance' measured at the non-linear load can be derived. At the non-linear load terminals, the harmonic currents created by the non-linear load can be related to the phase voltage at the non-linear load terminals using the relevant transmission line admittance and the phase voltage at the fault location.

$$\begin{cases} i_{anll} = (v_{a2} - v_{ax})Y_{T2} \\ i_{bnll} = (v_{b2} - v_{bx})Y_{T2} \end{cases} \tag{11}$$

Substituting (7) into (5), the phase voltages at the fault location are described in terms of the harmonic currents

flowing to the relevant phases.

$$\begin{cases} v_{ax} = \left(1 + \dfrac{Y_s + Y_1}{Y_{Tx}}\right) \dfrac{Ai_{anll} + Bi_{bnll}}{A^2 - B^2} \\ v_{bx} = \left(1 + \dfrac{Y_s + Y_1}{Y_{Tx}}\right) \dfrac{Bi_{anll} + Ai_{bnll}}{A^2 - B^2} \end{cases} \quad (12)$$

The phase voltage at the non-linear load terminal v_{a2}, v_{b2} can be expressed by substituting (12) into (11)

$$\begin{cases} v_{a2} = \left(1 + \dfrac{Y_s + Y_1}{Y_{Tx}}\right) \dfrac{(Ai_{anll} + Bi_{bnll})}{A^2 - B^2} + Z_{T2} i_{anll} \\ v_{b2} = \left(1 + \dfrac{Y_s + Y_1}{Y_{Tx}}\right) \dfrac{(Bi_{anll} + Ai_{bnll})}{A^2 - B^2} + Z_{T2} i_{bnll} \end{cases} \quad (13)$$

then the phase–phase voltage at the non-linear load terminal is derived and given as

$$v_{ab2} = \left\{ \left(1 + \frac{Y_s + Y_1}{Y_{Tx}}\right) \frac{1}{A + B} + Z_{T2} \right\} (i_{anll} - i_{bnll}) \quad (14)$$

In the frequency domain, the 'line–line self-impedance' at the non-linear load terminal at the third harmonic frequency can then be calculated using

$$\begin{aligned} Z_{ab2}(3\omega) &= \frac{F(v_{ab2})_{3\omega}}{F(i_{anll})_{3\omega}} \\ &= \cdots \left[\left(1 + \frac{Y_s(3\omega) + Y_1(3\omega)}{Y_{Tx}(3\omega)}\right) \right. \\ &\quad \left. \times \frac{1}{A(3\omega) + B(3\omega)} + Z_{T2}(3\omega) \right] \\ &\quad \times \cdots \left(1 - \frac{F(i_{anll})_{3\omega}}{F(i_{bnll})_{3\omega}}\right) \end{aligned} \quad (15)$$

It can be seen from (10), (15) and the variables A, B, that the 'line–line self-impedances' at the load terminals (including the passive load and the non-linear load) are a function of fault resistance and fault location. The characteristic indicates that these parameters can be used for identifying fault location if a fault occurs. If the line currents flowing to the loads via the load distribution centres are continuously monitored together with the line voltage, and the frequency spectra is analysed (for example by the REU), the triplen harmonics frequencies will increase, when a fault is present, providing a measurement which can be used to detect, and possibly locate faults.

3 Experimental validation

Simulation results presented in [22, 23] showed the effectiveness of line–line self-impedance at the third harmonic frequency for fault identification and detection. In this section, experimental results are presented to verify the new algorithm.

3.1 Experimental distribution system

The simplified laboratory representation of the aircraft distribution system described in [5] and simulated in [23, 24] was constructed as shown in Fig. 2. The experimental system circuit contains a programmable supply source, – the Chroma Programmable alternating current (AC) power source [26]–, which has a wide output frequency range (15–1 200 Hz) and the ability to generate a very clean AC output. There are also two passive resistive loads (6.8 and 8.0 Ω per phase) and a non-linear load – a three-phase capacitor-smoothed rectifier which supplies a resistive load of 6.0 Ω. The capacitor used for smoothing the output of the rectifier has a capacitance of 4.7 mF. The transmission cables are modelled by a lumped π-type circuit. The characteristic parameters used for the cables here are, a resistance of 0.02 Ω/m, an inductance of 0.8 μH/m and a capacitance of 0.12 nF/m with each section representing a cable of length 5.5 m. The parameters are typical of unshielded twisted tierce cables.

Faults are imposed between phase A and phase B, at any of the five node locations in the experimental circuit (denoted by the numbers 1–5) using the fault-control

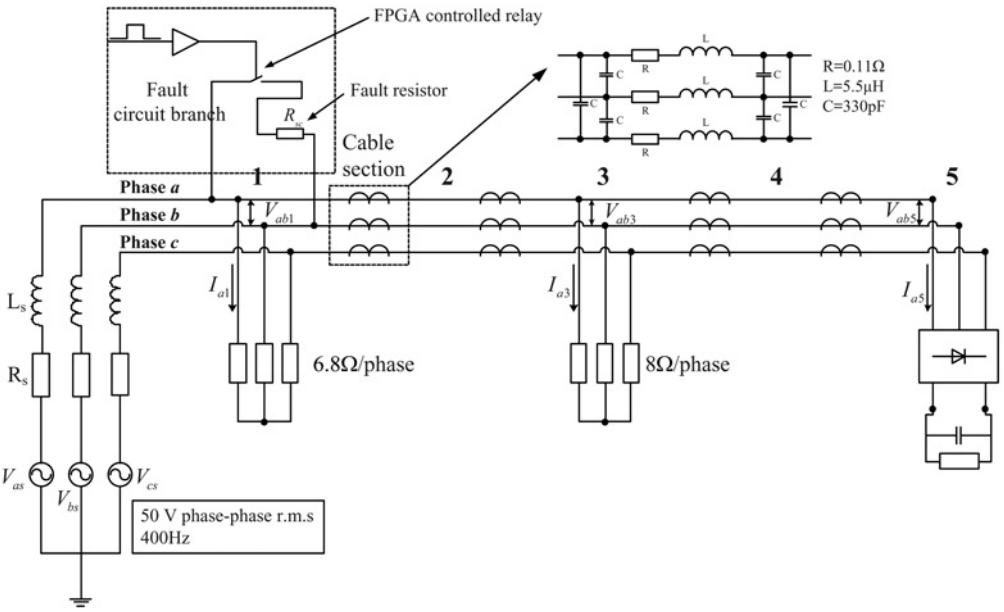

Fig. 2 *Experimental circuit*

doi: 10.1049/iet-est.2011.0051

Table 1 Equivalent THLSI (resistance, Ω) measured at each load terminal (Nodes 1, 3 and 5) for faults imposed at locations 1–5 consecutively with a known short-circuit resistance from 2 to 5 Ω

R_{sc}, Ω	Fault location 1			Fault location 2			Fault location 3			Fault location 4			Fault location 5		
	Node 1	Node 3	Node 5	Node 1	Node 3	Node 5	Node 1	Node 3	Node 5	Node 1	Node 3	Node 5	Node 1	Node 2	Node 5
2	8.16	11.10	−0.83	9.59	12.52	−0.96	10.27	13.15	−0.96	10.64	13.48	−0.88	10.05	13.01	−0.72
3	8.42	11.10	−0.80	9.74	12.72	−0.96	10.81	13.49	−0.98	10.79	14.10	−0.95	11.14	14.24	−0.87
4	8.55	11.10	−0.80	10.12	12.84	−0.95	10.81	13.53	−0.99	11.22	14.11	−0.97	11.58	14.64	−0.92
5	8.61	11.10	−0.79	10.14	12.84	−0.94	10.95	13.72	−0.99	11.46	14.11	−0.99	11.70	14.79	−0.94

circuit shown. The fault is triggered by the user from a bespoke FPGA-based data acquisition system, which also coordinates data capture and processing [27, 28]. All of the phase–phase node voltages and phase load currents are recorded. The system can be configured to impose a variety of different fault resistances. The test is initiated by the user and a trigger signal is sent to the analogue-to-digital converters to start recording data. After a scheduled duration d_1, in which the voltages and currents are recorded when the experimental circuit is in normal (pre-fault) operation, a trigger signal is sent to close the fault branch. The fault is imposed for a duration d_2, so that a sufficient post-fault data can be captured. The data recorded in the time duration d_1 is used to remove the effects of the 'background' harmonic distortion present during normal system operation from the post-fault data (d_2) to improve the impedance estimate at harmonic frequencies if required [23, 24]. The data recorded in the time duration d_2 are then used to calculate the equivalent 'line–line self-impedance' at each load centre at the third harmonic frequency for post-fault conditions. This is achieved by taking the Fourier transform of the measured voltage and load current at each node, and calculating (3) at the third harmonic frequency.

The fundamental frequency used in these experiments is 400 Hz and the line–line voltage is 50 V RMS. In successive experiments, faults are imposed at the five potential fault locations numbered as shown in Fig. 2. At each fault location, faults are imposed using different fault resistors and the resulting voltages and currents are recorded using a sampling frequency of 500 kHz. The value of the fault resistor can vary between 2 and 5 Ω.

3.2 Calibration of the system

This section presents the calibration of the experimental system. The aim of this section is to determine the third harmonic impedance as measured at each of the load nodes, for the known fault conditions. The fault condition is characterised by fault resistance and fault location. Once the system has been characterised, then unknown faults at unknown locations can be identified and located by coordinating the real-time measurements of third harmonic impedance at different load nodes.

The calibration was achieved by a series of tests, whereby, the third harmonic impedance was measured at different load nodes for different fault resistances (2, 3, 4 and 5 Ω) placed at different fault locations. The voltages and load phase currents at each load terminal were recorded for each test, so that the equivalent third harmonic impedances could be calculated offline. With this calibration data, listed in Tables 1 and 2, equivalent third harmonic impedance curves of fault resistance against fault locations measured at each load node (Nodes 1, 3 and 5) can be produced.

Table 2 Equivalent THLSI (reactance, Ω) measured at the non-linear load terminal (node 5) for faults imposed at locations 1–5 consecutively with a known short-circuit resistance from 2 to 5 Ω

R_{sc}, Ω	Fault location 1	Fault location 2	Fault location 3	Fault location 4	Fault location 5
2	−0.69	−0.72	−0.69	−0.60	−0.50
3	−0.74	−0.80	−0.79	−0.72	−0.64
4	−0.78	−0.86	−0.86	−0.81	−0.74
5	−0.80	−0.89	−0.90	−0.86	−0.81

The experimental system introduces measurement noise and rounding error; hence the experiments were repeated several times. The equivalent third harmonic impedances measured at each load node for a specific fault location are calculated by averaging the impedances estimated for five repeated experiments under the same fault condition. The averaged impedance values are taken as the mean values. The variations around the mean values are calculated using (16)

$$\sigma_i = \pm \left| \frac{\max(\text{abs}(Z_{\max,i}), \text{abs}(Z_{\min,i})) - Z_{\text{av},i}}{Z_{\text{av},i}} \right| \% \qquad (16)$$

where, σ_i is the variation around the impedance mean value calibrated at the load Node i, $Z_{\text{av},i}$ is the averaged impedance value calibrated at load Node i; $Z_{\max,i}$ is the maximum impedance value measured at load Node i during calibration, while $Z_{\min,i}$ is the minimum impedance value measured at load Node i. The maximum standard variation around the mean impedance values at the load nodes was found to be ±2.5%. This value was used to obtain error bars as shown in the graphs presented with the case studies. These variations make the decision-making procedure more complicated.

In the following subsections, different groups of unknown faults are imposed and identified using the calibrated third harmonic impedance curves of fault resistance against fault locations. A rheostat with a variable resistance up to 2.2 Ω was connected in series with one of the four known fault resistors, so that a fault with an intermediate resistance value can be imposed on the experimental network. This was considered to be an unknown fault.

3.3 Case studies

In this section, two groups of unknown faults were imposed and analysed. For the first group of unknown faults, six faults were imposed successively at location 5, but with different short-circuit resistances. These six resistances were 2.3, 2.7, 3.3, 3.7, 4.3 and 4.7 Ω, respectively. For the

Table 3 Equivalent THLSI measured at each load terminal for faults imposed at location 5 with six different short-circuit resistances

R_{sc}, Ω		2.3	2.7	3.3	3.7	4.3	4.7
Node 1 (resistance)		10.293	11.125	11.417	11.655	11.835	11.864
Node 3 (resistance)		13.128	14.121	14.241	14.559	14.608	14.645
Node 5	resistance	−0.751	−0.795	−0.877	−0.896	−0.925	−0.931
	reactance	−0.539	−0.625	−0.668	−0.716	−0.763	−0.799

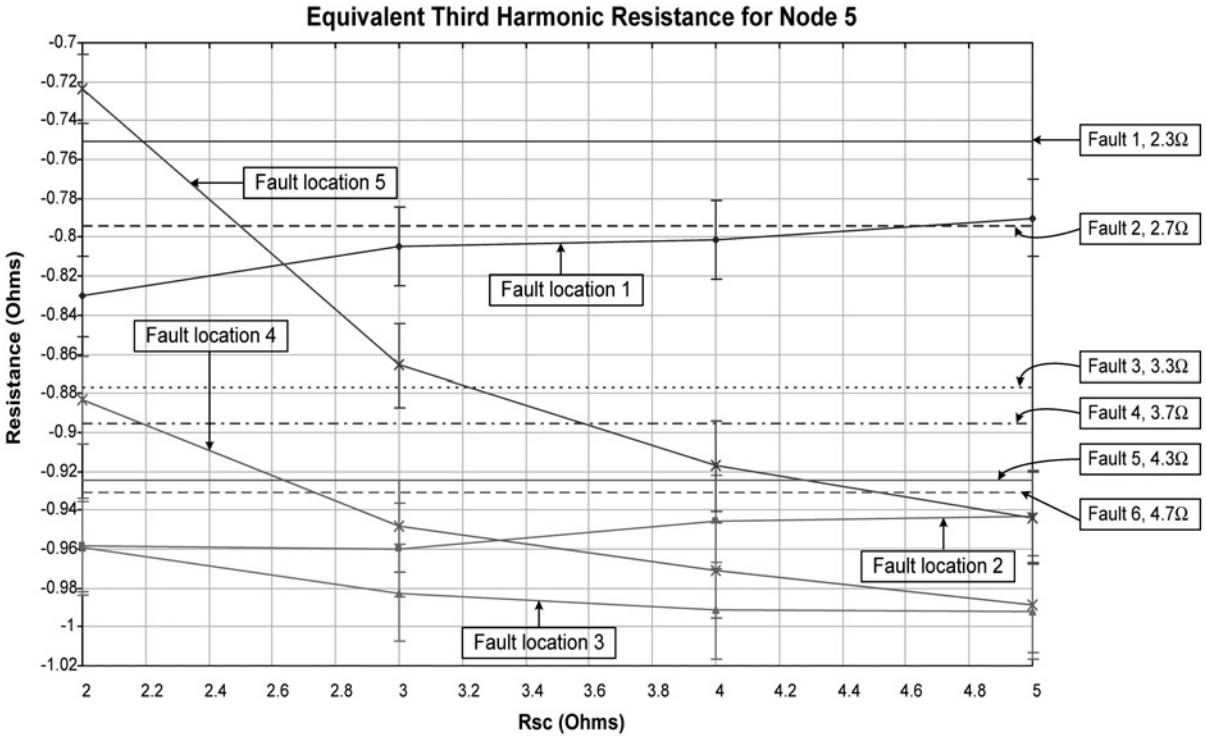

Fig. 3 *Equivalent third harmonic resistance curves measured at the rectifier (Location 5) for six different faults occurring at location 5*

second group of unknown faults, five faults were successively imposed at the five potential fault locations from locations 1 to 5 with the same fault resistance, 2.3 Ω. In this study, note that for Nodes 1 and 3, the reactance values were negligible.

3.3.1 Case 1 – different fault resistances: The equivalent third harmonic impedances measured at each load node are listed in Table 3 when the six faults occur successively at location 5. The decision making process uses calibrated curves for the third harmonic resistance and reactance measured at Node 5.

To illustrate the decision making process, the following description refers to Fig. 3. The solid lines denote the different calibration curves – the values from Table 3 – with estimated error range measured at Node 5 for different known faults and fault locations. The horizontal axis is the fault resistance varying from 2 to 5 Ω, denoted as R_{sc} (Ω). The different style horizontal lines (such as dotted, dash-dot, dash and solid) correspond to the third harmonic resistance measured at Node 5 when the unknown faults occur, as shown in Table 3.

The intersection of each dotted line with each solid line provides a potential solution for the identification of each unknown fault. For example, a measured resistance of −0.795 Ω (Fault 2) could indicate a fault resistance in the range of 2.6–5 Ω at fault location 1, or a fault resistance in the range of 2.2–2.8 Ω at fault location 5. The intersections for each measured third harmonic resistance for the unknown faults (Faults 1–6) with the calibrated third harmonic resistance curves for the different calibrated locations (FL1–FL5) are listed in Table 4. In Table 4, it can be seen that the first fault (Fault 1) has only one solution, which indicates that this fault occurs at location 5 with a fault resistance in the range 2–2.4 Ω. For the other faults, further information is required to identify each fault explicitly. The equivalent third harmonic reactance curves against fault locations measured at location 5 are plotted in Fig. 4 and use the same representation as in Fig. 3. The measured third harmonic reactances for the six unknown faults are also depicted by dotted lines in Fig. 4.

Table 4 Solutions for six faults using the equivalent third harmonic resistance curves against fault locations for the rectifier

Fault	Curve				
	FL1	FL2	FL3	FL4	FL5
Fault 1	–	–	–	–	2–2.4
Fault 2	2.6–5	–	–	–	2.2–2.8
Fault 3	–	–	–	2–2.4	2.8–3.6
Fault 4	–	–	–	2–2.6	3–4.2
Fault 5	–	3.8–5	–	2.2–3	3.6–5
Fault 6	–	3.4–5	–	2.2–3.4	3.6–5

doi: 10.1049/iet-est.2011.0051

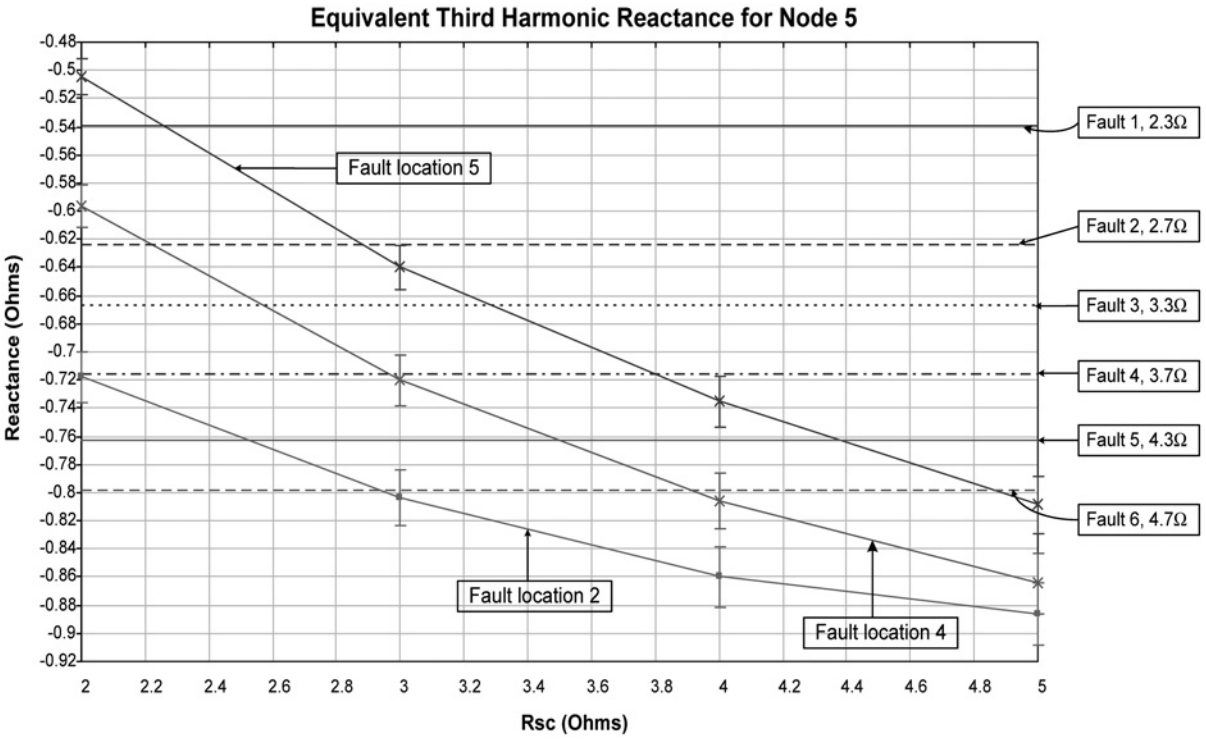

Fig. 4 *Equivalent third harmonic reactance curves measured at the rectifier (Location 5) for six different faults occurring at location 5*

The solutions for each fault, that is, the intersections between the dotted and solid curves of Fig. 4 are listed in Table 5. From Table 5, it is clear that the first and second faults (Faults 1 and 2) have a unique solution. Fault 1 occurred at location 5 with a fault resistance in the range of 2–2.4 Ω, which is consistent with the actual measured fault resistance. Fault 2 occurred at location 5 with a fault resistance in the range of 2.6–3 Ω. In combination with the solution given in Table 4, the range of the possible fault resistance values for Fault 2 was narrowed down to (2.6, 2.8 Ω), consistent with the actual fault resistance used (2.7 Ω). For Faults 3–6, further information is still needed to identify them explicitly. This is achieved by using the third harmonic impedance measured at the other load nodes. In an analogous way, the calibrated third harmonic resistance curves against fault location as measured at the passive loads (Node 1 and 3) can be presented with the equivalent third harmonic resistances for the four remaining unknown faults (Faults 3–6) which can be plotted as horizontal lines. Owing to space limitation, these figures are not presented here.

In Table 6 the solutions – the curve intersections – for the four unidentified faults are listed (Faults 3–6) using the calibrated third harmonic resistance curves measured at the passive load at Node 3. It is clear that Faults 4 – achieve unique solutions. It indicates that these three faults occur at location 5. Fault 4 occurs at location 5 with a fault resistance in the range of 2.8–5 Ω, Fault 5 occurs at location 5 with a fault resistance in the range of 3–5 Ω and Fault 6 occurs at location 5 with a fault resistance in the range of 4–5 Ω. The calibrated third harmonic resistance curves measured at the passive load at Node 1 are then used to identify the remaining unidentified faults. The solutions for Fault 3 are tabulated in Table 7.

For Fault 3, Tables 4–7 indicate that there are two solutions to the fault location, that is, location 4 and location 5. If this fault occurs at location 4, the solutions for

Table 5 Solutions for six faults using the equivalent third harmonic reactance curves against fault location for the rectifier

Fault	Curve			
	FL1	FL2	FL4	FL5
Fault 1	–	–	–	2–2.4
Fault 2	–	–	–	2.6–3
Fault 3	–	–	2.4–2.8	3–3.6
Fault 4	–	2–2.2	2.8–3.2	3.6–4
Fault 5	–	2.2–2.8	3.2–3.8	4–4.6
Fault 6	–	2.6–3.4	3.6–4.4	4.6–5

Table 6 Solutions for the four unidentified faults (Faults 3 to 6) using the equivalent third harmonic resistance curves against fault locations for the passive load at Node 3

Fault	Curve	
	FL4	FL5
Fault 3	2.6–5	2.6–4
Fault 4	–	2.8–5
Fault 5	–	3–5
Fault 6	–	3–5

Table 7 Solution for the one unidentified fault (Fault 3) using the equivalent third harmonic reactance curves against fault locations for the passive load at Node 1

Fault	Curve	
	FL4	FL5
Fault 3	3.4–5	3–5

Table 8 Equivalent third harmonic impedances measured at each load terminal for five faults imposed at five potential fault locations with the same fault resistance, 2.3 Ω

Fault conditions		Fault 1	Fault 2	Fault 3	Fault 4	Fault 5
Node 1 (resistance)		8.327	9.860	10.456	10.583	10.293
Node 3 (resistance)		11.073	12.610	13.323	13.483	13.128
Node 5	resistance	−0.827	−0.955	−0.951	−0.881	−0.751
	reactance	−0.713	−0.748	−0.715	−0.633	−0.539

Table 9 Solutions for five faults using the equivalent third harmonic resistance curves against fault locations for the rectifier

Fault	Curve				
	FL1	FL2	FL3	FL4	FL5
Fault 1	2–3	–	–	–	2.4–3
Fault 2	–	2–5	2–3	2.6–4.6	4.4–5
Fault 3	–	2–5	2–2.8	2.6–4.4	4.4–5
Fault 4	–	–	–	2–2.4	2.8–3.8
Fault 5	–	–	–	–	2–2.4

the fault resistance in each of the tables are (2, 2.4), (2.4, 2.8), (2.6, 5) and (3.4, 5) Ω for Tables 6–9, respectively. There is no common fault resistance for this set indicating that the fault did not occur at location 4. If this fault occurs at location 5, the solutions for fault resistance specified in each table are (2.8, 3.6), (3, 3.6), (2.6, 4) and (3, 5) Ω for Tables 6–9, respectively. The common fault resistance for these sets is (3, 3.6) Ω. This logical process indicates that this fault occurred at location 5 with a fault resistance range of (3, 3.6) Ω. By combining all the solutions tabulated in Table 4–7, all the six unknown faults were detected and correctly located at Node 5.

3.3.2 Case 2 – faults at different locations: In the second case study, five faults are successively imposed at the five potential fault locations from locations 1 to 5. Each time a fault resistance of 2.3 Ω was used. The equivalent third harmonic impedances measured for the 5 unknown faults at each load terminal are listed in Table 8.

The procedure to identify these five faults is implemented in an analogous way to Case 1. The calibrated third harmonic resistance curves against fault locations measured at Node 5 are shown again in Fig. 5, together with the measured third harmonic resistance for the five unknown faults (as measured at Node 5).

The intersections for each third harmonic fault resistance measured with the calibrated third harmonic resistance curves for each fault location are listed in Table 9. Only Fault 5 is identified unambiguously. The calibrated third harmonic reactance curves for each fault location as measured at Node 5 and the calibrated resistance curves as measured at Nodes 1 and 3 are required to identify clearly, the four unknown faults (Faults 1–4).

The calibrated third harmonic reactance curves at Node 5 are shown in Fig. 6 with the five faults of Case 2. The curve intersections are specified in Table 10.

By combining Tables 9 and 10, Fault 1 achieved a unique solution. Fault 1 occurred at location 1 with a fault resistance

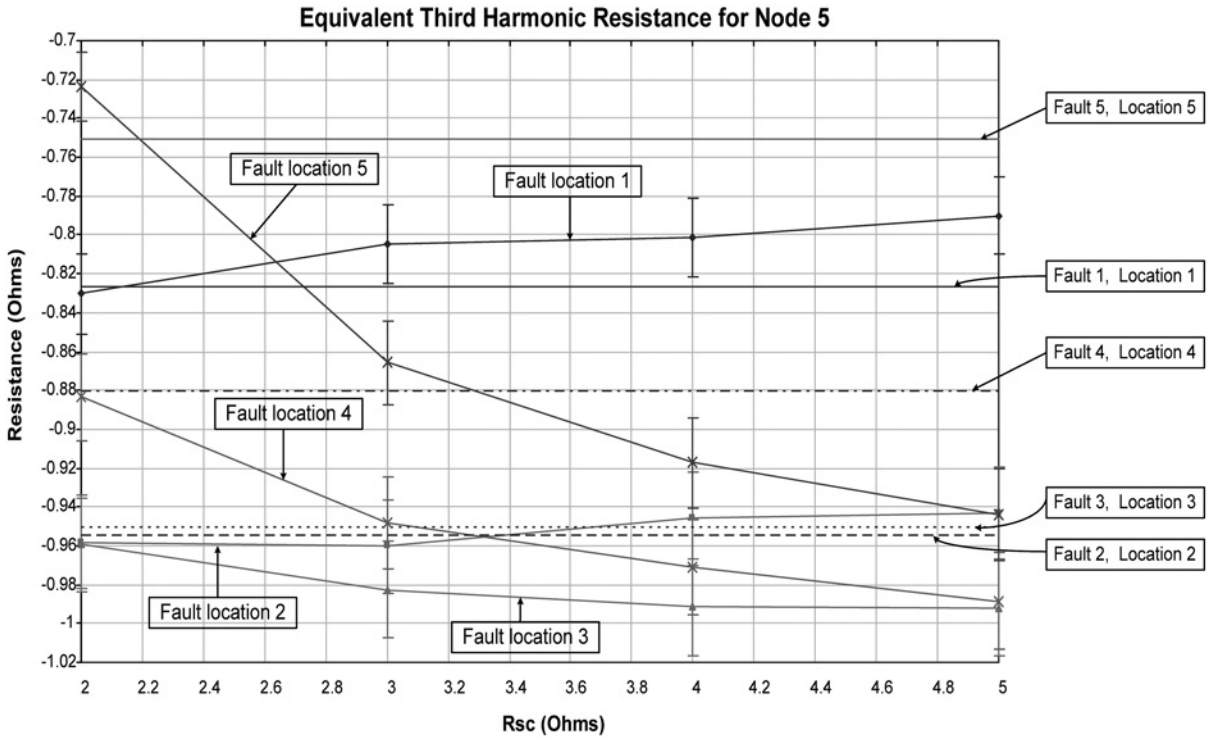

Fig. 5 *Equivalent third harmonic resistance curves against fault locations measured for rectifier's terminals (Location 5) with five faults occurring at the five potential fault locations with the same fault resistance 2.3 Ω*

doi: 10.1049/iet-est.2011.0051

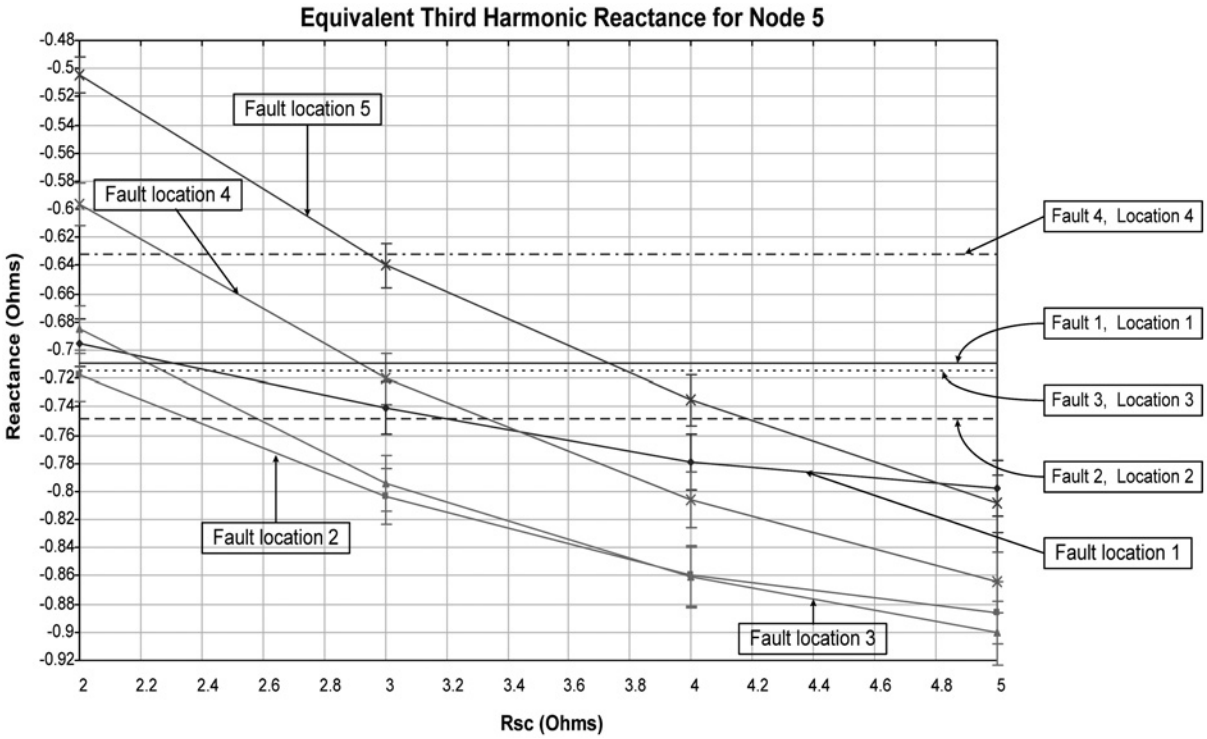

Fig. 6 *Equivalent third harmonic reactance curves against fault locations measured for rectifier's terminals (Location 5) with five faults occurring at the five potential fault locations with the same fault resistance 2.3 Ω*

Table 10 Solutions for five faults using the equivalent third harmonic reactance curves against fault locations for the rectifier

Fault	Curve				
	FL1	FL2	FL3	FL4	FL5
Fault 1	2–2.8	–	–	–	3.4–4
Fault 2	–	2–2.6	2.2–2.8	3–3.6	3.8–4.4
Fault 3	–	2–2.2	2–2.6	2.8–3.2	3.6–4
Fault 4	–	–	–	2–2.4	2.8–3.2

in the range of 2–2.8 Ω. The remaining three unidentified faults (Faults 2–4) need more information to unambiguously identify the fault locations. Similarly, the calibrated third harmonic resistance curves measured for the passive load at Node 3 can be easily reproduced with the three unidentified faults.

In an analogous way, the remaining unidentified faults can be analysed in combination with the calibrated third harmonic impedance curves (including resistance and reactance) measured for passive loads. The final solutions for these five unknown faults are listed in Table 11.

Table 11 Solutions for five unknown faults

Fault	Solution	
	Fault location	Fault resistance,Ω
Fault 1	location 1	2–2.8
Fault 2	location 2	2–2.6
Fault 3	location 3	2–2.6
Fault 4	location 4	2–2.4
Fault 5	location 5	2–2.4

The actual value of the fault resistance 2.3 Ω, is within the fault resistance range identified for each fault.

4 Discussion

The experimental results for the simplified system of the previous section demonstrated that by combining the information measured from different load distribution centres, a logical decision process can be executed which can determine the correct fault location and fault resistance for the experimental conditions. The method employed here calculates the 'line–line self-impedances' from the measured current and voltage by using a discrete Fourier transform algorithm. Data are captured for 20 cycles after the fault is imposed and the system reaches the steady state again and the impedances are at present calculated offline. In the experiments, a resistor and an inductor connected in series represent cables with a length of 5.5 m. The solutions for different unknown experimental faults indicate that the proposed approach can correctly distinguish faults occurring on cable sections. It can also be concluded that the fault location resolution is to be about 5.5 m in this experimental system. This approach demonstrates the viability of the line–line self-impedances as a parameter which can be used for cable condition monitoring, and that monitoring can be achieved by using current measurements normally available at load distribution centres, and by additional decision making logic within a central controller with little additional hardware cost. Although, this experimental rig is somewhat simplified compared with an actual aircraft distribution system, the studies of [23, 24] have shown that the principle can be applied if only the major load distribution centres are considered in a more complicated system, although a good knowledge of system layout is required. In this algorithm, the equivalent third harmonic

resistance curves depend on the load condition as well, but this should be known as the loads are continuously monitored in this system. Once the load condition changed and was known, the equivalent third harmonic impedance curves can be reproduced accordingly and the same identification procedure can be applied if any fault happens afterwards.

The actual implementation of the algorithm in a practical application needs further investigation. There is a trade-off between the speed of response and accuracy (and also false trips) which needs further consideration if this is to be applied directly for backup protection. Other algorithms may be better suited to fast, real-time decision making, for example, digital synchronous filters which can be used with a variable central frequency or a multi-rate filter bank [18], wavelets (although their real-time processing requirements are still large even if they reduce data capture times). These are currently under investigation. It has been noted already that the impedance measurements are small and can be corrupted by measurement and other noise, resulting in a low SNR. Error bounds can be incorporated into the calibration and decision making processes as appropriate. Moreover, if the data is used for fault location rather than fault detection, advanced signal processing algorithms as discussed could be used to improve the effective SNR and provide a more robust decision. Further work is required here to determine whether, statistical or probability based algorithms would enhance the decisions made for a hierarchical approach to condition monitoring and in-service maintenance.

The commissioning phase described in Section 3.2 outlines a complicated experimental approach to determine the third harmonic self-impedance curves used for fault detection. An alternative mathematical approach based on system configuration, and cable parameters has been derived and will be presented in a future publication. The basis of this approach extends from (9) and (14) exploiting the parameters A and B. The required information should be readily available for a particular aircraft distribution system, and the curves can potentially be recalculated online as the distribution is reconfigured for different loading arrangements.

5 Conclusions

A new fault location scheme has been proposed, which uses impedance estimation at the third harmonic frequency. The newly defined line–line impedance, as viewed from the load distribution points, does not have a direct physical meaning, although, it is dependent on the physical phase impedances of the system to some extent. They are also dependent on the ratios of the line currents involved in the calculation of the line–line impedance. In normal service, the system will contain low levels of triplen currents. When faults occur, the change of conduction mode of the rectifiers will result in the generation of triplen harmonics. Therefore the impedance at third harmonic frequency is used to detect and identify the fault location. The fault location is found by comparing the measured values during a fault with data obtained via a calibration process. This calibration needs to be performed with equipment in situ and is performed as part of the commissioning of the equipment or after the distribution system has been renovated. This may add complexity and time for aircraft construction, but the resultant benefits for system condition monitoring have the potential to be more than a compensation. This approach has advantages over artificial intelligence-based methods, such as neural networks, as the decisive process is transparent and verifiable.

The method has been validated by the experimental results. This proposed fault detection scheme using the THLSI can be applied to provide additional information to the primary protection system for accurately determining fault locations in order to take corresponding action. By using the measured load currents rather than the actual bus currents, it provides an independent approach to bus protection, which does not rely on bus current measurement.

6 References

1 Rosero, J.A., Ortega, J.A., Aldabas, E.: 'Moving towards a more electric aircraft', *IEEE Aerosp. Electron. Syst. Mag.*, 2007, **22**, (3), pp. 3–9
2 Moir, I., Seabridge, A.: 'Aircraft systems: mechanical, electrical, and avionics subsystems integration' (John Wiley & Sons, Chichester, 2008, 3rd edn.)
3 Emadi, K., Ehsani, M.: 'Aircraft power systems: technology, state of the art, and future trends', *IEEE Aerosp. Electron. Syst. Mag.*, 2000, **15**, (1), pp. 28–32
4 Pallett, E.H.J.: 'Aircraft electrical systems' (Longman Scientific & Technical, Wiley, London, New York, 1987)
5 McGoldrick, P.: 'More electric aircraft – power system proveder perspective'. Seminar Electrical Drive Systems for the More Electric Aircraft, UK Magnetics SocietySeminar, Bristol, April 2007
6 Avery, C.R., Burrow, S.G., Mellor, P.H.: 'Electrical generation and distribution for the more electric aircraft'. 42nd Int. Universities Power Engineering Conf., 2007. UPEC 2007., 2007
7 Bo, Z.Q.: 'A new non-communication protection technique for transmission lines', *IEEE Trans. Power Deliv.*, 1998, **13**, (4), pp. 1073–1078
8 Jiang, J.A., Ching-Shan, C., Chih-Wen, L.: 'A new protection scheme for fault detection, direction discrimination, classification, and location in transmission lines', *IEEE Trans. Power Deliv.*, 2003, **18**, (1), pp. 34–42
9 Wright, A., Christopoulos, C.: 'Electrical power system protection' (Chapman & Hall, 1993)
10 Cynthia Furse, You Chung Chung, Chet Lo, Praveen Pendayala: 'A critical comparison of reflectometry methods for location of wiring faults', *Smart Struct. Syst.*, 2006, **2**, (1), pp. 24–26
11 Steiner, J.P., Weeks, W.L.: 'Time-domain reflectometry for monitoring cable changes', 1990, Technical report, Electric Power Inst., Palo Alto, CA (USA), School of Electrical Engineering, Purdue Univ., Lafayette, IN (USA), p. 59
12 Furse, C., You Chung Chung, Dangol, R., Nielsen, M., Mabey, G., Woodward, R.: 'Frequency domain reflectometry for on-board testing of aging aircraft wiring', *IEEE Trans. Electromagn. Compat.*, 2003, **45**, (2), pp. 306–315
13 Griffiths, L.A., Parakh, R., Furse, C., Baker, B.: 'The invisible fray: a critical analysis of the use of reflectometry for fray location', *IEEE Sens. J.*, 2006, **6**, (3), pp. 697–706
14 Reis Jacklyn, Castro Agostinho, L.S., Costa João, C.W.A., Riu Jaume, R.I., Ericson Klas: 'Sequence and spread spectrum time domain reflectometry for transmission line analysis'. Broadband Access Communication Technologies II, SPIE, Boston, MA, USA, 2007
15 Sharma, C.R., Furse, C., Harrison, R.R.: 'Low-power STDR CMOS sensor for locating faults in aging aircraft wiring', *IEEE Sens. J.*, 2007, **7**, (1), pp. 43–50
16 Furse, C., Smith, P., Safavi, M., Chet Lo: 'Feasibility of spread spectrum sensors for location of arcs on live wires', *IEEE Sens. J.*, 2005, **5**, (6), pp. 1445–1450
17 Furse, C., Smith, P., Chet Lo, You Chung Chung: 'Spread spectrum sensors for critical fault location on live wire networks', *Struct. Control and Health Monit.*, 2005, **12**, (3–4), pp. 257–267
18 Smith, P., Furse, C., Gunther, J.: 'Analysis of spread spectrum time domain reflectometry for wire fault location', *IEEE Sens. J.*, 2005, **5**, (6), pp. 1469–1478
19 Borlase, S.H.: 'Advancing to true station and distribution system integration in electric utilities', *IEEE Trans. Power Deliv.*, 1998, **13**, (1), pp. 129–134
20 Apostolov, A.P.: 'Universal transmission line protection intelligent electronic devices'. Transmission and Distribution Conf. and Exposition, 2001 IEEE/PES, 2001

doi: 10.1049/iet-est.2011.0051

21 Giovanini, R., Coury, D.V., Hopkinson, K.M., Thorp, J.S.: 'A primary and backup cooperative protection system based on wide area agents', *IEEE Trans. Power Deliv.*, 2006, **21**, (3), pp. 1222–1230
22 Qian, Z., Sumner, M., Thomas, D.: 'Fault detection for aircraft power systems using the impedance at third harmonic frequency'. IET Ninth Int. Conf. on Developments in Power System Protection, 2008. DPSP 2008, 2008
23 Qian, Z., Sumner, M., Thomas, D.: 'Fault detection for the aircraft distribution systems using impedance estimation'. Fourth IET Conf. on Power Electronics, Machines and Drives, 2008. PEMD 2008, 2008
24 Sakui, M., Fujita, H., Shioya, M.: 'A method for calculating harmonic currents of a three-phase bridge uncontrolled rectifier with DC filter', *IEEE Trans. Ind. Electron.*, 1989, **36**, (3), pp. 434–440
25 Sakui, M., Fujita, H.: 'Calculation of harmonic currents in a three-phase convertor with unbalanced power supply conditions', *IEE Proc. B*, 1992, **139**, (5), pp. 478–484
26 Chroma Programmable 3-Phase AC Source, Model 61700 Series, Chroma ATE INC
27 Coggins, D., Thomas, D.W.P., Hayes-Gill, B.R., Yiqun Zhu: 'An FPGA based travelling wave fault locator'. Int. Conf. on Filed-Programmable Technology, Kitakyushu, Japan, 2007
28 Coggins, D., Thomas, D.W.P., Hayes-Gill, B.R., Yiqun Zhu, Pereira, E.T., Cabral, S.H.L.: 'A new high speed FPGA based travelling wave fault recorder for MV distribution systems'. Ninth Int. Conf. on Developments in Power System Protection, Glasgow, UK, 2008